Measuring the ionization balance of gold in a low-density plasma of importance to inertial confinement fusion[1]

M.J. May, P. Beiersdorfer, G.V. Brown, K.B. Fournier, M. Gu, S.B. Hansen, M. Schneider, J.H. Scofield, S. Terracol, K.J. Reed, B. Wilson, K.L. Wong, K.R. Boyce, R. Kelley, C.A. Kilbourne, and F.S. Porter

Abstract: Charge state distributions (CSDs) have been determined in low-density ($\approx 10^{12}$ cm^{-3}) gold plasmas having either a monoenergetic beam ($E_{\mathrm{Beam}} = 2.66$, 3.53, 4.54, 5.35, 5.85, and 6.35 keV) or experimentally simulated thermal electron distributions ($T_{\mathrm{e}} = 2.0$, 2.5, and 3.0 keV). These plasmas were created in the Livermore electron beam ion traps, EBIT-I and EBIT-II. Line emission and radiative recombination features of K to Kr-like gold ions were recorded in the X-ray region with a crystal spectrometer and a photometrically calibrated microcalorimeter. The CSDs in the experimentally simulated thermal plasmas were inferred by fitting the observed $4f \rightarrow 3d$ and $5f \rightarrow 3d$ lines with synthetic spectra from the Hebrew University Lawrence Livermore Atomic Code (HULLAC). Additionally, the CSDs in the beam plasmas were inferred both from fitting the line emission and fitting the radiative recombination emission to calculations from the General Relativistic Atomic Structure Program. Despite the relatively simple atomic physics in the low-density plasma, differences existed between the experimental CSDs and the simulations from several available codes (for example, RIGEL). Our experimental CSD relied upon accurate electron impact cross sections provided by HULLAC. To determine their reliability, we have experimentally determined the cross sections for several of the $n = 3 \rightarrow 4$ and $n = 3 \rightarrow 5$ excitations in Ni to Ga-like Au and compared them to distorted wave calculations. Cross-section calculations by flexible atomic code (FAC) and HULLAC were found to be very consistent. Recent Au spectra recorded during experiments at the OMEGA laser facility are presented and compared with those recorded from EBIT-I and EBIT-II. This comparison shows that spectra from the two sources are surprisingly similar despite a 10 order of magnitude difference in their respective plasma densities.

PACS Nos.: 52.50.Fs, 52.25.Jm, 34.80.Kw, 34.80.Lx

Résumé : Nous avons déterminé les distributions des états de charge (CSDs) dans des plasmas d'or de basse densité ($\approx 10^{12}$ cm^{-3}) qui ont soit un faisceau monoénergétique ($E_{\mathrm{Beam}} = 2{,}66$, 3,53, 4,54, 5,35, 5,85 et 6,35 keV) soit des distributions d'électrons à excitation thermique expérimentalement simulées ($T_{\mathrm{e}} = 2{,}0$, 2,5 et 3,0 keV). Ces plasmas ont été générés dans les pièges ioniques à faisceau d'électrons à Livermore, dans EBIT-I et EBIT-II. Les caractéristiques des lignes d'émission et des recombinaisons radiatives ont été enregistrées dans la région X à l'aide d'un spectromètre à cristal et d'un microcalorimètre calibré photométriquement. Les CSDs dans les plasmas expérimentalement simulés ont été déduites par ajustement numérique aux lignes $4f \rightarrow 3d$ et $5f \rightarrow 3d$ observées avec un spectre synthétique obtenu du logiciel de calculs atomiques Hebrew University-Lawrence Livermore (HULLAC). De plus, les CSDs dans le faisceau de plasma ont été déduites par ajustement numérique à la fois des lignes d'émission et de l'émission de recombinaison radiative pour des calculs à l'aide du programme General Relativity Atomic Structure. Malgré la relative simplicité de la physique atomique dans le plasma de faible densité, des différences existent entre les CSDs expérimentaux et celles de diverses simulations (par exemple RIGEL). Nos valeurs expérimentales de CSD reposent sur des sections efficaces d'impact électronique précises fournies par HULLAC. Afin de cerner leur fiabilité, nous avons déterminé expérimentalement les sections efficaces pour plusieurs excitations $n = 3 \rightarrow 4$ et $n = 3 \rightarrow 5$ dans des ions d'or de types Ni et Ga et les comparons à des calculs utilisant des ondes déformées. Nous observons que les sections efficaces calculées avec FAC et HULLAC sont en bon accord. Des spectres récents d'Au enregistrés par le montage expérimental laser OMEGA sont comparés avec ceux obtenus de EBIT-I et EBIT-II. Cette comparaison montre que les spectres de ces deux sources sont étonnamment similaires, malgré les 10 ordres de grandeur de différence en densité.

[Traduit par la Rédaction]

Received 14 March 2007. Accepted 4 June 2007. Published on the NRC Research Press Web site at http://cjp.nrc.ca/ on 9 February 2008.

M.J. May,[2] P. Beiersdorfer, G.V. Brown, K.B. Fournier, M. Gu, S.B. Hansen, M. Schneider, J.H. Scofield, S. Terracol, K.J. Reed, B. Wilson, and K.L. Wong. Lawrence Livermore National Laboratory, L-95, Livermore, CA 94550, USA.
K.R. Boyce, R. Kelley, C.A. Kilbourne, and F.S. Porter. NASA-Goddard Space Flight Center, Code 662, Greenbelt, MD 20700, USA.

[1] Paper given at the Workshop on Twenty Years of Spectroscopy with EBIT held in Berkeley, California, 13–15 November 2006.
[2] Corresponding author (e-mail: may13@llnl.gov).

 doi: 10.1139/P07-150

1. Introduction

Predicting the correct charge state distribution (CSD) is critical for understanding the radiation levels, energy deposition, energy balance, etc. of high-temperature plasmas such as those produced inside Z-pinches [1, 2], tokamaks [3, 4], astrophysical objects [5], and hohlraums irradiated by intense lasers [6, 7]. However, models that calculate the CSDs are far from adequate for predicting the charge state distribution in a nonlocal thermodynamic equilibrium (NLTE) plasma. This inadequacy has been strikingly illustrated in a comparison of NLTE calculations of the CSDs of several elements [8]. The calculations for high-Z elements at the conditions of typical laser-produced plasmas had the most significant discrepancies. For example, the predicted average charge state, $\langle q \rangle$, for gold at a temperature, T_e, of 2.5 keV and a density, n_e, of 10^{20} cm^{-3} varied from +43 to +63! Some progress has been made in improving the consistency of the calculations as detailed in a more recent paper by Bowen et al. [9] in which the predicted charge state of Au at the same conditions was ∼47 with a variation of roughly ±5. However, some of the other plasma conditions exhibit larger differences. The CSD calculations for models in Bowen et al. were guided by several definitive experiments [10–13] that inferred the CSD of Au in different conditions. It is evident that experiments using different conditions are needed to test the implementation of the atomic physics processes in the models.

In particular, low-density plasmas (for example, those in an EBIT) have fewer active relevant processes (for example, no photoionization, opacity, three-body recombination, etc.) and also provide less complicated experiments than the high-density ones. Any inferred CSD from a laser-produced plasma relies on the calculated collisional excitation cross sections from the atomic structure codes. Measurements in EBIT plasmas can be used to measure the collision excitation cross sections directly and compare them to theory. Thus, removing one uncertainty in the CSD determinations. In addition, since spectral features recorded from an EBIT plasma can be unambiguously identified in both charge state and transition, they can be used to interpret and identify emission features in the very complex gold emission spectra from laser-produced plasmas.

Three experiments have inferred the CSD of Au in different high-density plasmas heated by the NOVA and the OMEGA laser. Foord et al. [10] inferred the charge state balance of a heated gold microdot buried in a Be foil at $n_e = 6 \times 10^{20}$ cm^{-3} and $T_e = 2.2$ keV in steady state by comparing the measured $5f \rightarrow 3d$ spectrum with atomic physics calculations. The experimental average ionization state, $\langle q \rangle$, $= +49.3 \pm 0.5$ was in reasonable agreement with the modeled value of +49.1 from RIGEL [15]. RIGEL is a super configuration-based collisional-radiative code that solves for a CSD by using Monte-Carlo techniques. To reproduce the experiment properly, two-electron processes such as dielectronic recombination (DR) were included in the modeling of the charge balance and the line intensities. In the second experiment, Glenzer et al. [11] measured the average gold ion charge state to be $+52 \pm 1$ in a fusion hohlraum plasma with a T_e of 2.6 keV, an n_e of 1.4×10^{21} cm^{-3} and a T_{rad} of 210 eV. The predicted steady state $\langle q \rangle = +50.5$, which was also calculated by RIGEL, was just outside the experimental error bar. Glenzer indicated that nonsteady-state kinetics might be a possible explanation of the discrepancy. The third experiment by Heeter et al. [12] measured the ionization balance of well-characterized NLTE gold plasmas with and without external radiation fields at electron densities near 10^{21} cm^{-3} and various electron temperatures spanning the range 0.8–2.4 keV. Time- and space-resolved M-shell gold emission spectra were analyzed using a sophisticated collisional-radiative model with hybrid level structure, finding average ion charges $\langle Z \rangle$ ranging from 42 to 50. At the lower temperatures, the spectra exhibited significant sensitivity to external radiation fields and included emission features from complex N-shell ions not previously studied at these densities. The analysis of all of these high density experiments was complicated by the transient nature and the many competing atomic processes present in the laser-produced plasma.

To support the more complex laser-produced plasma experiment, spectra were recorded from steady-state Au plasmas created in the Livermore electron beam ion traps EBIT-I and EBIT-I [13]. These plasmas had either monoenergetic beams or experimentally simulated thermal electron distributions at electron densities of $\approx 10^{12}$ cm^{-3}. Many collisionally excited (CE) lines from $n = 4 \rightarrow 3$, $5 \rightarrow 3$, $6 \rightarrow 3$, and $7 \rightarrow 3$ X-ray transitions from K-like to Kr-like gold ions between 1500 and 5000 eV for the monoenergetic beam and simulated Maxwell–Boltzmann plasmas were recorded. The radiative recombination (RR) emission from roughly Ni-like to Kr-like gold ions was observed between 5000 and 8500 eV for some of the monoenergetic beam plasmas. The spectra were recorded by employing both a photometrically calibrated X-ray microcalorimeter (XRS) [16] and an X-ray crystal spectrometer [17]. Unambiguous identifications have been made and accurate photon energies have been measured for 140+ of Ni-like to Kr-like Au transitions [14].

The CSDs in the monoenergetic beam and the experimentally simulated thermal plasmas were inferred by comparing the X-ray CE line intensities with atomic physics calculations from the Hebrew University Lawrence Livermore Atomic Code (HULLAC) [18]. Additionally, the CSDs in the beam plasmas were inferred by comparisons of the RR features to modeling from the General Relativistic Atomic Structure Program (GRASP) [19, 20]. These measurements observed the ionization balance in steady state conditions. Despite the fewer active processes in the coronal plasma, the inferred CSDs from EBIT-I and EBIT-II disagree with the results from the available modeling codes for both monoenergetic beam and experimentally simulated thermal plasmas.

Here, we review the measurements and present data obtained at a simulated electron temperature of 2.5 keV and a monoenergetic beam plasma having an energy of 4.54 keV. The predicted $\langle q \rangle$ for the simulated thermal plasma having an electron temperature of 2.5 keV differed by as much as four charge states from the experimental value. The difference in the $\langle q \rangle$ was less that one charge state for the plasma having an $E_{beam} = 4.54$ keV, however, the other beam energies had larger discrepancies. These experiments have been used to further the analysis of laser-produced plasma experiments.

The inferred CSDs from spectra recorded in any gold plasma rely upon accurate electron impact cross sections provided by the atomic physics code (for example, HULLAC). To determine their reliability, we have experimentally determined the cross sections for the $3d \rightarrow 4$f and $3d \rightarrow 5f$ excitations in Ni-like to Ga-like Au and compared them to theory. Results for the transitions in Ni-like are presented.

2. Plasmas at the Livermore EBITs

Gold plasmas were created in EBIT-I and EBIT-II by successive electron collisional ionization of low-charged ions introduced into the trap from a metal vacuum vapor ion source [21]. Radial trapping of the ions in the electron mode [22] was achieved by the electrostatic attraction of the electron beam. Two end drift tubes, which have a positive bias of a few hundred volts with respect to a center drift tube, confined the ions axially along the beam. Plasmas having either a monoenergetic electron beam or an experimentally simulated thermal electron distribution were utilized to obtain the data presented here. More details of the experiments can be found in refs. 13 and 14.

The monoenergetic electron beam plasmas created in EBIT-I and EBIT-II had energies, E_{beam}, of 2.66, 3.53, 4.54, 5.35, 5.85, and 6.35 ± 0.04 keV. The reported beam energies are corrected for the space charge effects of a beam current of ≈55 mA [23] for the 2.66, 3.53, and 4.54 beam energies and ≈150 mA for the 5.35, 5.85, and 6.35 keV beam energies. The electron beam had a Gaussian electron energy distribution with a full width half maximum of ≈50 eV. The plasmas with experimentally simulated thermal electron distributions had temperatures, T_{e}, of 2.0, 2.5, and 3.0 ± 0.04 keV. The reported temperatures include the space charge correction for ≈40 mA of beam current. To create these plasmas, the electron beam energy and anode voltages were swept to map out a Maxwell–Boltzmann (MB) electron distribution in time by using the techniques described in refs. 24 and 25. In each sweep, the time spent at an electron beam energy was proportional to the experimentally simulated temperature's MB electron distribution probability at that energy. The beam energy was swept between electron energies of a few hundred eV to 5 or 8 times the temperature value of the plasma. With these voltages the majority of the MB distribution was sampled. Concurrently, the anode voltage was swept to maintain a constant density in the electron beam. Each MB sweep, which lasted 5 ms, was continuously repeated until the end of the trapping cycle. The spectra presented here for both types of plasmas were taken during the steady-state portion of the trapping cycle (i.e., after the CSD has reached its equilibrium value). This was ≈1 s after the start of the beam energy being studied or the MB sweep and lasted for 8 to 12 s before the trap was emptied. Each experimental condition required repeating the trapping cycle at the same conditions for ≈12 h to record sufficient signal on the spectrometers.

The X-ray crystal spectrometer recorded in first order the high-resolution spectra of the $5f \rightarrow 3d$ and the $4f \rightarrow 3d$ transitions of Kr-like to K-like gold ions between photon energies of 3100–4300 eV and 2400–3200 eV, respectively. For these measurements, two Si(111) crystals with lattice spacings of $2d = 6.2712$ Å were used. Each crystal was used to measure a different spectral range simultaneously. The gas counter detectors were filled with ≈1 atm of P10 gas and had either a 4 μm thick polypropylene or 1 μm thick polyimide window. In addition, each window was coated with a 100–200 Å thick Al layer. A vacuum isolation window composed of 0.5 μm of polyimide was located between the crystal spectrometer and EBIT-I or EBIT-II. The energy resolution was ≈5.0 eV at 3300 eV and ≈2.5 eV at 2500 eV. The absorption of the gas including the Ar K edge at 3210 eV and the transmission efficiency of the windows were taken into account when the experimental spectrum was compared with the modeling results.

Fig. 1. A raw X-ray microcalorimeter spectrum observed in an EBIT-I plasma having an E_{beam} of 5.35 keV.

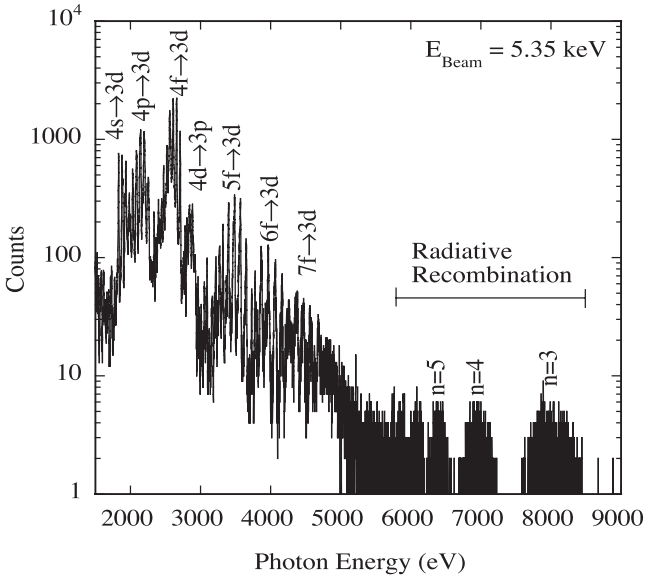

The XRS microcalorimeter recorded gold CE lines between 1500 and 5000 keV and RR features from 5000 to 8500 keV. A sample raw spectrum is shown in Fig. 1 for a plasma having $E_{\mathrm{beam}} = 5.35$ keV. This plasma contains ionization stages from about Cu to Cr-like Au. The XRS detector head consisted of an array of ion-implanted thermistors with a 8.5 μm thick HgTe photon absorber. The thermistors directly measured the temperature change of a single photon absorbed by the HgTe. To measure the small changes in temperature, the detector head was cooled to an operating temperature of 59 mK by an adiabatic demagnetization refrigerator mounted inside a Dewar filled with super-fluid helium. Since each absorber–thermistor must be recooled after each photon event, the maximum count rate was limited to ≈100 counts/s across the entire array. This count rate is well suited for astrophysical observation and the typical low photon fluxes from EBIT-I and EBIT-II. Two XRS detector front-end assemblies have been used at the Livermore EBITs. The first array read out 30 active pixels and had a spectral resolution of ≈12 eV. The current version reads out 16 pixels and had a resolution of 8–10 eV for these measurements.

3. Modeling

The HULLAC [18] atomic data package was used to calculate the atomic structure, transition rates, and synthetic line intensities for the Ni-like to Kr-like Au ions. The radiative transition rates and energy level structure of each ionization state were calculated from the Dirac equation with a parametric potential. Electron impact excitation cross sections, σ_{CE}, were calculated semi-relativistically in the distorted wave approximation. Details of the CE modeling are discussed in refs. 13, 14.

Due to the low electron density of the trapped ions, the modeling only addresses transitions that are fed primarily through collisional excitation from the ground level. All possible $n = 4 \rightarrow 4$ and $n = 3 \rightarrow 4$ to $3 \rightarrow 7$ excitations from the ground state to singly excited configurations were included for Ni to Ga-like ions. The models for the Ge to Kr-like ions contained only the $n = 4 \rightarrow 4$, $n = 3 \rightarrow 4$, and $3 \rightarrow 5$ excitations. The

Co- to K-like ions models contained only the $n = 3 \rightarrow 4$ and $3 \rightarrow 5$ excitations. When only the line intensities were desired, the level populations of each ionization state were coupled with only the adjacent, higher charged ion. The model for the higher charged ion included fewer levels than the lower charged ion and was only considered to include the effect of dielectronic recombination on the collisionally excited transitions. Dielectronic recombination rate coefficients were found by requiring detailed balance with the HULLAC autoionization rates. When a CSD was computed from HULLAC, smaller models of the charge states from Ni-like to Kr-like Au, which did not include all the high-n transitions (and were not used for the spectral analysis) were coupled together and run until a steady-state solution was reached. CSDs were calculated for the plasmas having an E_{beam} of 2.66, 3.53, and 4.54 keV and a T_e of 2.0 and 2.5.

The rate coefficients and the radiative transition probabilities were put into a collisional-radiative matrix. The level populations were calculated by solving the coupled set of equations:

$$\frac{dn_j}{dt} = 0 = \sum_i n_i R_{i\rightarrow j} - n_j \sum_i R_{j\rightarrow i}$$

where n_i is the relative population of level i of a given ion, $R_{j\rightarrow i}$ is the rate at which the population transfers from level j to level i (which can be in the adjacent ionization state). All electric and magnetic dipole and quadrupole radiative transitions and relevant magnetic octopole transitions were included. In the EBIT-I and EBIT-II plasmas, collisional electron excitation from the ground level or metastable levels was the only significant process populating the upper levels.

Synthetic spectra were produced for detailed comparisons and fitting to the XRS and crystal spectra from both the monoenergetic beam plasmas and thermal plasmas. The relative emissivity, $J_{i\rightarrow j}$, for each transition within an ionization state was calculated for either a MB temperature or a Gaussian electron distribution with $\Delta E_{\text{FWHM}} = 50$ eV at $n_e = 1 \times 10^{12}$ cm^{-3}.

GRASP [19] simulated the RR features for comparison with the spectra recorded by the XRS from the beam plasmas. GRASP is an atomic structure code that determines the bound state radial wave functions by numerically solving the multiconfiguration Dirac–Fock functions. Modifications of the code [20] produce the matrix elements and the cross sections for the continuum processes of RR and dielectronic recombination. GRASP provides cross sections that account for the polarization effects in our EBITs. The free-bound RR rates are calculated with more accuracy than are need for the experiments and are assumed to have no error.

4. Comparison with laser plasmas

The measured spectra from laser-produced plasmas can be very complex. Many competing processes can contribute to the line intensities (for example, opacity, three-body recombination, etc). The unambiguous identification of a transition from a spectrum and its assignment to the correct ionization state can be very challenging. The problem can be compounded if the spectral resolution is significantly degraded by source broadening of the target [29]. Accurate photon-energy measurements and line identifications of spectra taken at EBIT-I and EBIT-II can significantly aid in this analysis. In addition, the measured line intensities can be directly compared with the laser-produced plasma spectra.

Fig. 2. (*a*) Au spectrum recorded from a gold halfraum heated by the OMEGA laser at LLE. Line identifications were done by comparisons with the spectrum from EBIT. (*b*) Au spectrum from an EBIT-I plasma having E_{beam} of 5.85 keV recorded by the crystal spectrometer.

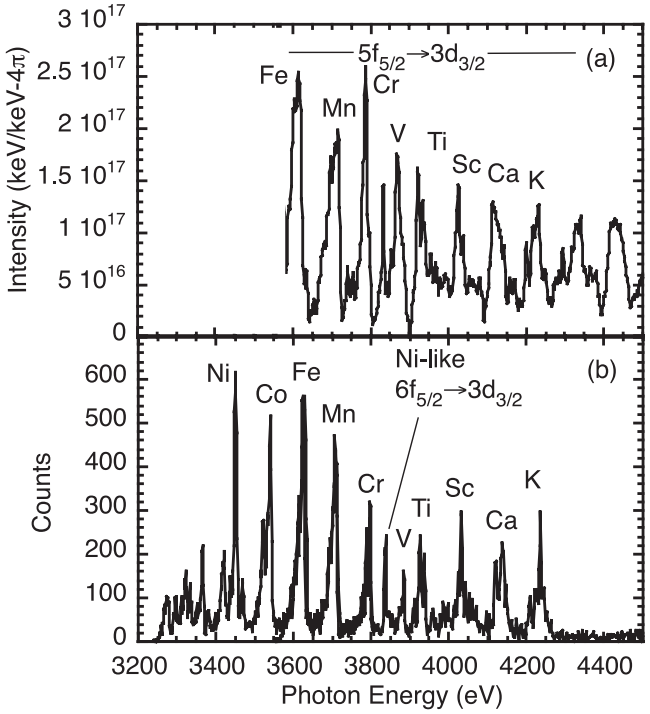

In EBIT-I and EBIT-II plasmas, the beam energy is user selectable allowing a specific set of gold ionization states to be isolated in the trap for analysis. For instance, the $E_{\text{beam}} = 4.54$ keV plasma is near the calculated ionization threshold of Ni-like gold at 4.89 keV but well above the threshold to ionize Cu-like into Ni-like at 2.96 keV. Therefore, Ni-like Au is the dominant ion in the trap and produces the most intense emission lines. By appropriately adjusting the beam energy, the charge distribution in the trap was shifted to ions as low as Kr-like and as high as K-like for the experiments detailed here. Unambiguous line identifications and accurate photon-energy measurements were done for many collisionally excited transitions through comparisons with HULLAC modeling for Kr to Ni-like Au. The uncertainty in the photon energies was ≈0.5 eV using the crystal spectrometer [14]. Photon-energy measurements are still in progress. Approximately 140 Ni to Kr-like lines have been identified.

A spectrum of the $5f \rightarrow 3d$ transitions from a monoenergetic beam plasma having $E_{\text{beam}} = 5.85$ keV in EBIT-I is shown in Fig. 2*b*. This identified and calibrated spectrum was taken with the crystal spectrometer at a spectral resolution of ≈7 eV. A spectrum in the same photon-energy region recorded from a Au halfraum heated by the OMEGA laser is shown in Fig. 2*a*. A Henway [30] convex crystal spectrometer recorded the spectrum at OMEGA with a similar spectral resolution to the one recorded at EBIT. Despite a difference of about 10 orders of magnitude in density, the two spectra are very similar in the limited range of the eight overlapping charge states

Fig. 3. Gold emission spectrum produced by a 2.5 keV experimentally simulated Maxwell–Boltzmann temperature. Broken lines are the HULLAC fits that are used to infer the CSD.

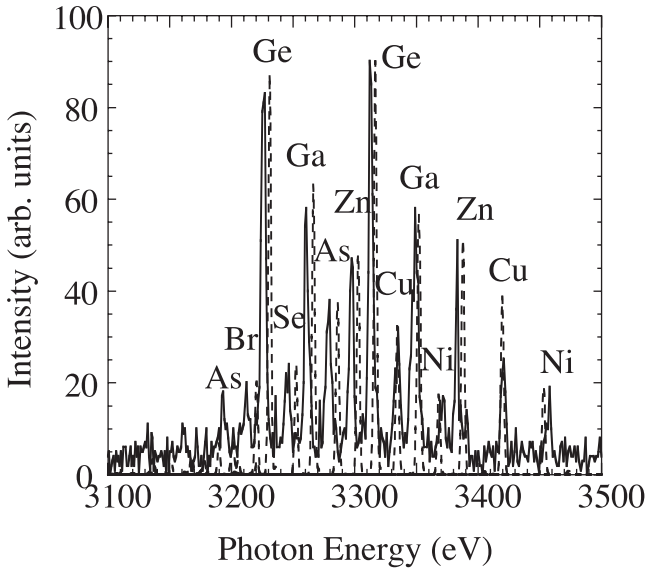

measured in both plasmas. The reason for the similarity can be understood by the fact that electric-dipole allowed transitions excited by electron impact collisions dominate both plasmas. The radiative decay rates are so fast that their emission is unperturbed by collisional or auto-ionization processes and thus the electrons predominately repopulate the same lower level in both cases. The identification and analysis of the OMEGA spectrum was much simplified by direct comparison with the fairly well-understood low-density spectrum.

5. Charge state distributions

The CSDs from EBIT-I and EBIT-II plasmas with the experimentally simulated MB electron distributions were determined by individually fitting the individual intensities of the $5f \rightarrow 3d$ and $4f \rightarrow 3d$ emission lines of each charge state with simulated spectra from the HULLAC atomic data package. The $5f \rightarrow 3d$ and $4f \rightarrow 3d$ line groups were fit separately. The measured and fit $5f \rightarrow 3d$ spectra from the $T_e = 2.5$ keV plasma is shown in Fig. 3. The $T_e = 2.5$ keV plasma is presented here since its conditions are the most relevant to the laser-produced experiments afore mentioned. The HULLAC fits (broken lines) include the corrections for the spectrometer photometric sensitivity. The HULLAC X-ray transition energies do not match the measured energies but differ by 3–10 eV, which illustrates the accuracy of the transition energy calculations. The resulting experimentally inferred CSDs from the $4f \rightarrow 3d$ and $5f \rightarrow 3d$ transitions from this plasma are shown in Fig. 4. Each point is the ionic fraction derived from the fit of the HULLAC intensities to one or two lines. The error that brackets each point included the statistical error from the counts in the spectral lines and the uncertainty in the fit to the line or lines in each charge state. The line intensities calculated by HULLAC are assumed not to have any intrinsic error. The experiment is compared with the simulations from the available modeling codes: RIGEL/MCXSN [15], RIGEL/ENRICO, and the Multiple Ion-

Fig. 4. Comparison of the gold charge state distributions at 2.5 keV determined from EBIT-II to the results from RIGEL/MCXSN, RIGEL/ENRICO and MIST. The lines are only added to guide the eye in the EBIT-II data. The dip at Kr-like ion in the MIST charge balance is due to the inclusion of the excitation–autoionization rates of Mitnik et al. [31] missing in the lower charge states.

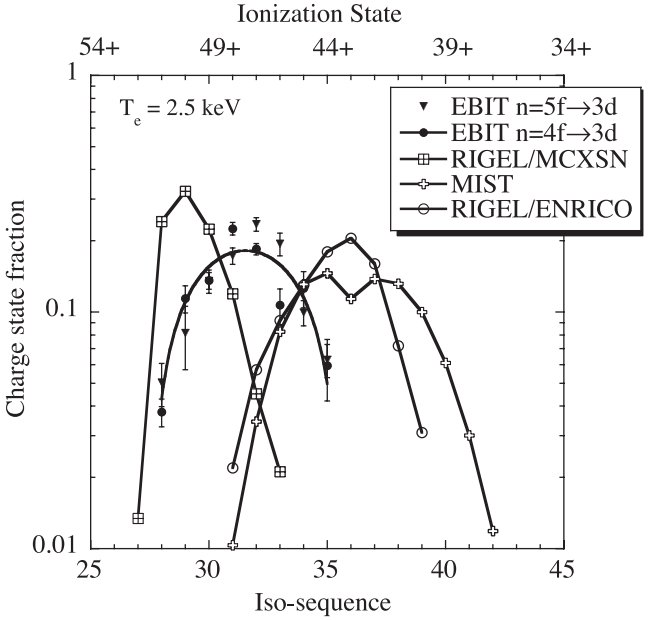

ization State Transport (MIST) [27] code. RIGEL is typically used for high-density laser-heated plasma experiments and is a super configuration-based collisional-radiative code that solves for a CSD by using Monte-Carlo techniques. MCXSN generates atomic physics rates for RIGEL based on hydrogenic supershells. ENRICO solves the Dirac equation explicitly to compute the RR and Auger processes. The collisional processes are calculated using generalized formulas. MIST is a low-density (10^{12} to 10^{14} cm^{-3}) tokamak impurity transport code and utilized the average ion model for the basis of its atomic physics rates [28]. Inclusion of the excitation–autoionization rates of Mitnik et al. [31] in MIST for charge states more highly ionized than Kr-like ions produced the dip in the charge balance at Kr-like Au (see Fig. 4) . All three of the calculations were run with $n_e = 1 \times 10^{12}$ cm^{-3} and $T_e = 2.5$ keV. The calculations bracket the experiment that had a $\langle q \rangle$ of 47.1 ± 0.4. This is the average from both the $n = 5 \rightarrow 3$ and $n = 4 \rightarrow 3$ spectral analysis. MIST predicted a lower average charge state by four. RIGEL/MCXSN and RIGEL/ENRICO predicted a higher and lower average charge state by three ions, respectively. Even with the better implementation of atomic physics in RIGEL/ENRICO, good agreement with the experimental CSD is not obtained. The CSD from the $T_e = 2.5$ keV EBIT plasma is shown in detail here, however, a similar result is found for the $T_e = 2.0$ keV EBIT plasma.

The CSD from the beam plasmas was determined by two separate methods. First, the $5f \rightarrow 3d$ and $4f \rightarrow 3d$ lines were fit with the HULLAC synthetic spectrum in a manner similar to that described for the experimentally simulated thermal plasmas. Second, the RR features were fit with simulations of the RR emission from GRASP. The RR spectrum for a monoenergetic Au plasma at $E_{Beam} = 4.54$ keV is shown in Fig. 5. The

Fig. 5. Radiative recombination spectrum measured by the calibrated X-ray microcalorimeter in a plasma with an $E_{\text{Beam}} = 4.54$ keV. The radiative recombination features are fit with calculations from the General Relativistic Atomic Structure Program to infer the charge state distributions.

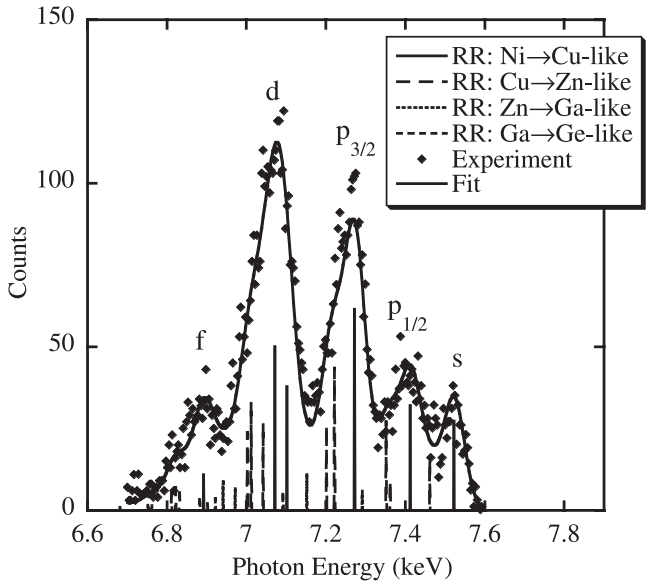

Fig. 6. Charge state distributions inferred from both the $5f \rightarrow 3d$, $4f \rightarrow 3d$ and fitting with HULLAC calculations and the radiative recombination spectrum and fitting with General Relativistic Atomic Structure Program calculations.

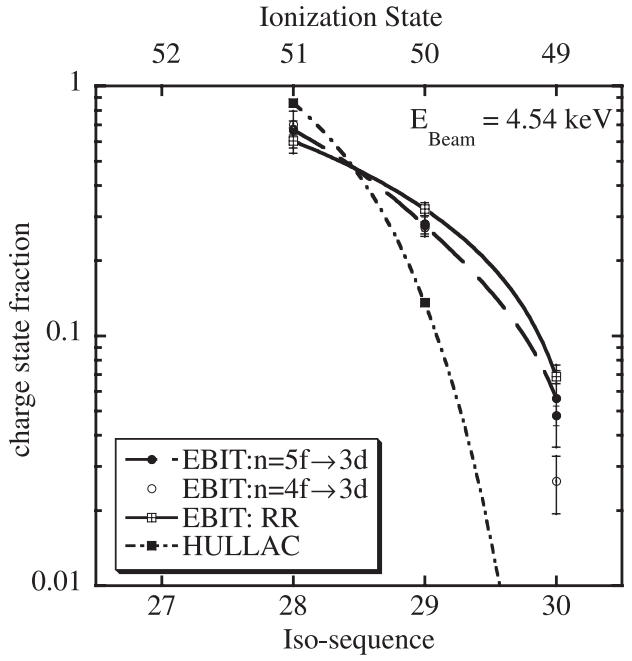

recombination of Ni → Cu, Cu → Zn, Zn → Ga, and Ga → Ge were seen from the continuum into the $n = 4s$, $4p_{1/2}$, $4p_{3/2}$, $4d$, and $4f$ sublevels. In the beam plasma, the RR features appear as lines with widths equal to the FWHM of the Gaussian electron energy distribution. The energy of the "line" is equal to the beam energy plus the energy of recombination from the continuum into the final state. The inferred CSDs from both the fits to the RR and the CE emission are shown for this plasma in Fig. 6. Both methods of inferring the CSD are very consistent. The $\langle q \rangle$ from the CE lines is 50.6 ± 0.9 and is consistent with the $\langle q \rangle$ of 50.5 ± 1.0 from the RR features. The CSD from the CE lines is the average from both the $n = 5 \rightarrow 3$ and $n = 4 \rightarrow 3$ spectra. RIGEL does not calculate CSDs for beam plasmas. Instead, HULLAC was used to calculate a CSD as described in Sect. 3. The CSD predicted by HULLAC (Labeled "HULLAC" in Fig. 6) did not agree with experiment. However, the $\langle q \rangle$ of 50.9 was reasonably close. To understand a plasma both the $\langle q \rangle$ and the CSD must be predicted properly.

6. Collisional excitations cross sections

The CSD from any Au plasma inferred from spectral fitting of the collisionally excited lines, directly depends on the accuracy of the electron impact collisional excitation cross sections, σ_{CE}, provided by the atomic structure codes (for example, HULLAC). To determine the accuracy of the calculations, absolute cross-section measurements of the $3d \rightarrow 4f$ and $3d \rightarrow 5f$ excitations in Ni-like to Ga-like Au were done in EBIT-I and EBIT-II [32]. Details of the method can be found in ref. 33. The total cross sections were determined from the intensities of the CE lines and RR emission recorded by the XRS in the beam plasmas using the formula

$$\sigma_{\text{CE}} = \frac{\sum_j G_j^{\text{RR}} \eta_j^{\text{RR}} T_j^{\text{RR}} \sigma_j^{\text{RR}}}{G^{\text{CE}} \eta^{\text{CE}} T^{\text{CE}}} \frac{I^{\text{CE}}}{I^{\text{RR}}}$$

The sum, j, is over the fine-structure levels. The intensities, I, are determined from the fits of the CE and RR features explained above. The variables η and T are the XRS detector efficiency and filter transmissions, respectively. The CE lines and RR features from EBIT-I and EBIT-II plasma are polarized. The polarization, P, is accounted for in the determination of the cross sections. The variable, G, is the angular distribution of the polarization, and $G = 3/(3 - P)$ for a dipole transition at 90°. Polarization is a function of the magnetic sublevel cross sections, which were calculated using a relativistic distorted wave code (DWS) [34]. For the Ni-like $3d_{3/2} \rightarrow 5f_{5/2}$ excitation having $J = 1 \rightarrow 0$, $P = (\sigma_{-1} - 2\sigma_0 + \sigma_{+1})/(\sigma_{-1} + 2\sigma_0 + \sigma_{+1})$. The polarization is ≈0.3 at a $E_{\text{Beam}} = 4.54$ keV.

The calculated total cross sections from several atomic data packages for the Ni-like $3d \rightarrow 4f$ and $3d \rightarrow 5f$ excitations are compared with the measured values in Fig. 7. The theoretical cross sections from HULLAC (broken lines) are consistent with those from DWS and the Flexible Atomic Code (FAC) [35]. The points are the measured cross sections. The error bars on each point included the statistical error from the counts in the spectral line and RR features, the uncertainty in the fits to the line or RR features in each charge state, and the uncertainty in the XRS photometric calibration. The $3d_{5/2} \rightarrow 5f_{7/2}$, $3d_{3/2} \rightarrow 5f_{5/2}$, and $3d_{3/2} \rightarrow 4f_{5/2}$ experimental cross sections are in good agreement with the calculations. The experimental cross sections for the $3d_{5/2} \rightarrow 4f_{7/2}$ excitation is ≈1.5 times the theory. For the Ni-like transitions, the excitation energy is below the ionization energy of the ion. This is not true for lower ionization states than Ni-like Au. For Cu-like Au, the energy required for the $3d \rightarrow 5f$ excitations is greater than the ionization energy of Cu-like at 2.96 keV. Thus, the upper states in Cu-like Au and lower charged ions have a branching ratio for auto-ionization

Fig. 7. Measured collisional excitation cross sections for $3d \rightarrow 4f$ and $3d \rightarrow 5f$ transitions in Ni-like Au and comparisons to several different distorted wave calculations.

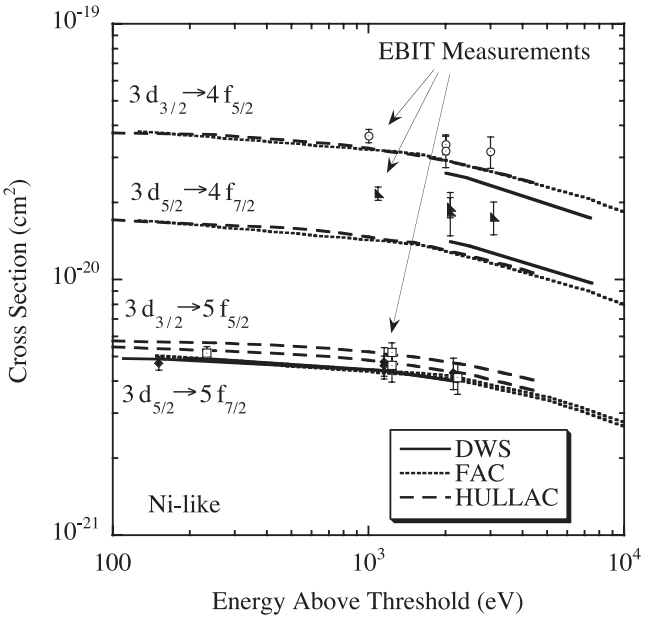

that must be included in the determination of the cross sections. Without this correction, the measured cross sections measurement will be slightly low. The branching ratio for radiative decay has been computed with FAC to be $B(5f_{5/2} \rightarrow 3d_{3/2}) = 0.832$ and $B(5f_{7/2} \rightarrow 3d_{5/2}) = 0.8$ for Cu-like Au. The energy required for the $3d \rightarrow 4f$ excitations are less than the ionization energy and require no corrections. Our measurement demonstrates that some (isolated) errors exist in the calculations of excitation cross sections. However, these were not enough to appreciably change the inferred CSD using HULLAC.

7. Conclusion

The gold CE line and RR emission have been recorded from monoenergetic beam plasmas ($E_{\mathrm{Beam}} = 2.66$, 3.53, 4.54, 5.35, 5.85, and 6.35 keV) and simulated thermal plasmas ($T_{\mathrm{e}} = 2.0$, 2.5, and 3.0 keV) created in EBIT-I and EBIT-II.

We have unambiguously identified approximately 140 emission lines of Ni-like to Kr-like Au in the 1.5 to 5 keV X-ray region and have accurate measurements of their photon energies. These calibrated and identified low-density gold spectra are very useful in the analysis of gold spectra recorded in laser-produced plasmas. The CSDs for the beam plasmas in our EBITs have been determined by fitting CE and the RR spectra with HULLAC synthetic spectra and GRASP RR calculations, respectively. The CSDs for plasmas with experimentally simulated thermal electron distributions were determined solely from fitting the CE spectra with HULLAC modeling. At a given condition, the different analysis from the experiments (for example, RR and CE from $5 \rightarrow 3$ and $4 \rightarrow 3$) yielded similar CSDs. However, the available modeling codes do not adequately reproduce the measurements. The experimental $\langle q \rangle$ for the simulated thermal plasma having an electron temperature of 2.5 keV differed by as much as four charge states from the predicted value. The smallest discrepancy was found in the beam plasma having $E_{\mathrm{beam}} = 4.54$ keV. The difference was less than one charge state between the experimental and predicted $\langle q \rangle$. However, the individual fractions at $E_{\mathrm{beam}} = 4.54$ keV varied by more than a factor of two. A more recent calculation by Peyrusse [36] has better agreement with the experiment through a refinement of the treatment of superconfigurations. To improve agreement with experimental measurements at laser-plasma densities, we are developing computationally tractable hybrid M-shell models that combine the accuracy of the fine-structure calculations with the completeness of superconfiguration models [37]. Finally, collisional excitation cross sections have been measured for the $3d \rightarrow 4f$ and $3d \rightarrow 5f$ excitations in Ni- to Ga-like Au . There is reasonable agreement between the measured and calculated cross sections. However, some discrepancies do exist.

Acknowledgements

This work was performed under the auspices of the US DOE by the University of California Lawrence Livermore National Laboratory under contract W-7405-ENG-48.

References

1. K.L. Wong, P.T. Springer, J.H. Hammer, C.A. Iglesias, A.L. Osterheld, M.E. Foord, H.C. Bruns, and J.A. Emig. Phys. Rev. Lett. **80**, 2334 (1998).
2. A.L. Velikovich, J. Davis, V.I. Oreshkin, J.P. Apruzese, R.Q. Clark, J.W. Thornhill, and L.I. Rudakov. Phys. Plasmas **8**, 4509 (2001).
3. C. De Michelis and M. Mattioli. Rep. Prog. Phys. **47**, 1233 (1984).
4. J.E. Rice, J.L. Terry, K.B. Fournier, M.A. Graf, M. Finkenthal, M.J. May, E.S. Marmar, W.H. Goldstein, and A.E. Hubbard. J. Phys. B: At. Mol. Opt. Phys. **29**, 2191 (1996).
5. J.C. Raymond and N.C. Brickhouse. Astrophy. Space Sci. **237**, 321 (1996).
6. H.R. Griem. Phys. Fluids B, **4**, 2346 (1992).
7. J. Lindl. Phys. Plasmas, **2**, 3933 (1995).
8. R.W. Lee, J.K. Nash, and Y. Ralchenko. J. Quant. Spectrosc. Radiat. Transfer, **58**, 737 (1997).
9. C. Bowen, R.W. Lee, and Yu. Ralchenko. J. Quant. Spectrosc. Radiat. Transfer, **99**, 102 (2006).
10. M.E. Foord, S.H. Glenzer, R.S. Thoe, K.L. Wong, K.B. Fournier, B.G. Wilson, and P.T. Springer. Phys. Rev. Lett. **85**, 992 (2000).
11. S.H. Glenzer, K.B. Fournier, B.G. Wilson, R.W. Lee, and L.J. Suter. Phys. Rev. Lett. **87**, 045002 (2001).
12. R.F. Heeter, S.B. Hansen, P. Beiersdorfer M.E. Foord, K.B. Fournier, D.H. Froula, A.J. Mackinnon, M.J. May, M.B. Schneider, and B.K.F. Young. *In* Proceedings of Atomic Processes in Plasmas. *Edited by* J.S. Cohen, S. Mazevet, and D.P. Kilcrease. American Institue of Physics, Melville, New York. 2004. p. 103.
13. K.L. Wong, M.J. May, P. Beiersdorfer, K.B. Fournier, B. Wilson, G.V. Brown, P. Springer, P.A. Neill, and C.L. Harris. Phys. Rev. Lett. **90**, 235001 (2003).
14. M.J. May, K.B. Fournier, P. Beiersdorfer, H. Chen, and K.L. Wong. Phys. Rev. E, **68**, 036402 (2003).
15. B.G. Wilson, J.R. Albritton, and D.A. Liberman. Radiative properties of hot dense matter. *Edited by* W. Goldstein, C. Hooper, J. Gauthier, J. Seely, and R. Lee. World Scientific, Singapore. 1991.

16. F.S. Porter, M.D. Audley, P. Beiersdorfer, K.R. Boyce, R.P. Brekosky, G.V. Brown, K.C. Gendreau, J. Gygax, S. Kahn, R.L. Kelley, C.K. Stahle, A.E. Szymkowiak. Proc. SPIE, **4140**, 407 (2000).
17. G.V. Brown, P. Beiersdorfer, and K. Widmann. Rev. Sci. Instrum. **70**, 280 (1999).
18. A. Bar-Shalom, M. Klapisch and J. Oreg. J. Quant. Spectrosc. Radiat. Transfer, **71**, 169 (2001).
19. F.A. Parpia, C.F. Fischer, and I.P Grant. Comput. Phys. Commun. **94**, 249 (1996).
20. J.H. Scofield. Phys. Rev. A, **9**, 3054 (1989).
21. I.G. Brown, J.E. Galvin, R.A. MacGill, and R.T. Wright. Appl. Phys. Lett. **49**, 1019 (1986).
22. P. Beiersdorfer, L. Schweikhard, J. Crespo López-Urrutia, and K. Widmann. Rev. Sci. Instrum. **67**, 3818 (1996).
23. M.A. Levine, R.E. Marrs, J.R. Henderson, D.A. Knapp, and M.B. Schneider. Phys. Scr. **22**, 157 (1988).
24. D.W. Savin, P. Beiersdorfer, S.M. Kahn, B.R. Beck, G.V. Brown, M.F. Gu, D.A. Liedahl, and J.H. Scofield. Rev. Sci. Instrum. **71**, 3362 (2000).
25. D.W. Savin, N.R. Badnell, P. Beiersdorfer, B.R. Beck, G.V. Brown, P. Bryans, T.W. Gorczyca, M.F. Gu, S.M. Kahn, J.M. Laming, D.A. Liedahl, W. Mitthumsiri, J.H. Scofield, and K.L. Wong. Can. J. Phys. **86** (2008). This issue.
26. R. Marrs, P. Beiersdorfer, and D. Schneider. Phys. Today, **47**, 27 (1994).
27. R.A. Hulse, Nucl. Technol. Fusion, **3**, 259 (1983).
28. D.E. Post, J.V. Jensen, C.B. Tartar, W.H. Grasberger, and W.A. Lokke. Atom. Data Nucl. Tables, **20**, 397 (1977).
29. M.J. May, M.B. Schneider, H.K. Chung, and D.E. Hinkel. UCRL-JRNL-214752 (2005).
30. L. Koppel and J. Eckels. Lawrence Livermore National Laboratory Report, UCRL-79781 (1977).
31. D. Mitnik, P. Mandelbaum, J.L. Schwob, A. Bar-Shalom, J. Oreg, and W.H. Goldstein. Phys. Rev. A, **50**, 4911 (1994).
32. M.J. May, P. Beiersdorfer, N. Jordan, J.H. Scofield, K.J. Reed, S.B. Hansen, K.B. Fournier, M.F. Gu, G.V. Brown, F.S. Porter, R. Kelley, C.A. Kilbourne, and K.R. Boyce. Nucl. Instrum. Methods Phys. Res. B, **235** 231 (2005).
33. H. Chen, P. Beiersdorfer, J.H. Scofield, K.C. Gendreau, K.R. Boyce, G.V. Brown, R.L. Kelley, F.S. Porter, C.K. Stahle, A.E. Szymkowiak, and S.M. Kahn. Astrophys. J. **567**, L169 (2002).
34. H.L. Zhang, D.H. Sampson, and R.E.H. Clark. Phys. Rev. A, **41**, 198 (1990).
35. M. Gu. Astrophys. J. **582**, 1241 (2003).
36. O. Peyrusse, C. Bauche-Arnoult, and J. Bauche. J. Phys. B, **38**, L137 (2005).
37. S.B. Hansen, J. Bauche, C. Bauche-Arnoult, and M.F. Gu. High Energy Density Phys. **3**, 109 (2007).